International Journal of Heat and Mass Transfer 149 (2020) 119186

Contents lists available at ScienceDirect

International Journal of Heat and Mass Transfer

journal homepage: www.elsevier.com/locate/hmt

Free convection in a trapezoidal enclosure divided by a flexible partition

S.A.M. Mehryan[a], Mohammad Ghalambaz[b,c,*], Reza Kalantar Feeoj[d], Ahmad Hajjar[e], Mohsen Izadi[f]

[a] Young Researchers and Elite Club, Yasooj Branch, Islamic Azad University, Yasooj, Iran
[b] Department for Management of Science and Technology Development, Ton Duc Thang University, Ho Chi Minh City, Vietnam
[c] Faculty of Applied Sciences, Ton Duc Thang University, Ho Chi Minh City, Vietnam
[d] Department of Mechanical Engineering, Shahrekord University, Shahrekord, Iran
[e] LabECAM, ECAM Lyon, Université de Lyon, Lyon, France
[f] Mechanical Engineering Department, Faculty of Engineering, Lorestan University, Khorramabad, Iran

ARTICLE INFO

Article history:
Received 5 October 2019
Revised 17 November 2019
Accepted 7 December 2019
Available online 17 December 2019

Keywords:
Fluid-Structure Interaction (FSI)
Trapezoidal enclosure
Flexible partition
Moving mesh technique
Finite element method

ABSTRACT

The Fluid-Structure Interaction (FSI) approach was utilized to model the displacement of a flexible partition in a trapezoidal enclosure due to interaction with an internal natural convection flow. A moving mesh technique, Arbitrary Lagrangian–Eulerian (ALE) method, is adopted to model the partition displacement and the flow and heat transfer in the enclosure. The finite element method is employed to solve the governing equations after transforming into a non-dimensional form. The effect of various non-dimensional parameters such as Rayleigh number, Prandtl number, trapezoidal walls inclination angles, and non-dimensional Young's modulus. The results show that the increase of Rayleigh number increases the heat transfer in the enclosure and the tension in the partition. Notably, raising *Ra* from 10^4 to 10^7 can increase the heat transfer rate in the cavity by 8 times. The inclination angle of cavity walls induces a minimal effect on the induced tensions in the partition while it influences the heat transfer. In particular, heat transfer rate in a square cavity is 15% higher than in a trapezoidal cavity having side walls with 30° angle of inclination.

1. Introduction

In recent years, natural convection heat transfer has attracted the attention of many researchers. This topic is divided into internal and external flows. Due to its engineering importance, natural convection heat transfer in the enclosures has attracted a large number of studies in this field. Therefore, various issues related to the natural convection heat transfer inside the cavities have been investigated. It can be referred to some scientific published works such as Ghalambaz et al. [1,2], Izadi et al. [3,4], and Mehryan et al. [5]. The heat transfer in cavities concerning entropy generation [6,7], porous cavity [8], conjugate heat transfer [9], nanofluids [10–12], and magnetohydrodynamic heat transfer [13] has been investigated in recent works.

Fluid-Structure Interaction (FSI) is a general issue, in which flexible structures are interacting with the surrounding fluid or with internal flows. These issues also play a vital role in many engineering applications. FSI topics are inherently complex because they are time-dependent and nonlinear. The vibration of the tubes in heat exchangers, solar energy collectors, shaking of airplane wings, wind turbine blades, feeding airbags of an automobile, ship motion, filtration process, pumping blood by heart, blood flow through veins, are only some of the applications. On the other hand, there are many engineering issues related to the classification of enclosures containing flexible walls or baffles such as electronic elements and industrial blades.

The study of the FSI combined with natural convection inside different shapes of enclosures has been the subject of some of the recent literature studies. Using a flexible thermal conductive membrane, Jamesahar et al. [14] studied the unsteady natural convective problem inside an enclosure. The influence of the fluid and the membrane properties on natural convection were considered. Ghalambaz et al. [15] considered an FSI approach to address an elastic fin, inserted to a hot wall of a cavity. The reported that an increase in the amplitude of the oscillating fin shows a positive effect on the heat transfer rate. They also calculated the best flexible fin length for heat transfer enhancement. Raisi and Arvin [16]

* Corresponding author at: Ton Duc Thang University, Ho Chi Minh City, Vietnam
E-mail address: mohammad.ghalambaz@tdtu.edu.vn (M. Ghalambaz).

https://doi.org/10.1016/j.ijheatmasstransfer.2019.119186
0017-9310/

examined a deformation of a flexible baffle, which was posited at the center of a square enclosure by employing the FSI approach. The results show that depending on the Rayleigh number and the system flexibility, the baffle length has different effects on the thermal conditions. Saleh et al. [17] solved time-dependent convection inside a cavity including a circular cylinder and two inserted elastic fins. A little amplitude oscillation has considerable effect on the heat transfer rate.

Using the FEM, Alsabery et al. [18] performed an FSI study to investigate the effect of the presence of a pliable oscillating fin inserted on the bottom wall of a cavity. Some of the key parameters such as left wall heater length, the thermal conductivity ratio, non-dimensional Young's modulus, dimensionless time, oscillating amplitude were considered. The results indicate the fluid flow and heat transfer significantly affected by the pliable oscillating fin.

Some of the literature studies tried to improve the heat transfer in cavities by using nanofluids or altering the geometry of enclosures. For instance, Aly and Raizah [19] performed an analysis on the natural convection of nanofluids in a wavy porous enclosure. The fluid flows and heat transfer were influenced by the motion of the particles inside a wavy enclosure. An increase in the volume fraction of nanoparticles slightly enhanced heat transfer through the cavity. Numerical calculation of natural convection around heated inclined plates was studied by Guha et al. [20]. The impacts of magnetic field and corrugated elastic walls on mixed convection of a nanofluid inside a cavity were numerically analyzed by Selimefendigil and Öztop [21]. They reported both of deterioration and enhancement of average Nusselt number with augmenting Hartman number.

The partitioned enclosure has many applications in various industries, including electronics, chemicals, and energy. For example, partitioned enclosures containing electronic components are applicable for cooling purposes, electric, or magnetic shielding. Some thermal storages are divided into partitions for better performance and mechanical reasons. In the chemical industries, divided reactors form separate sections for different chemical reactions. Also from the practical perspective of using partitions in the cavities, many researchers have investigated the natural convection heat transfer in these partitioned enclosures [22–26]. Acharya and Jetli [27] reported a key task of thermal stratification between the cold wall and the discriminant. At low Ra, the tendency to separation of the flow behind the divider is reported whereas, at high Ra, stratification is remarkable and creates the flow to sequester from the cold wall creating a dissociation head-on the discriminant.

Tong and Gerner [28] analyzed the Natural convection heat transfer inside divided rectangular cavities filled by air. They reported the greatest reduction in heat transfer by placing a partition in the middle of the cavity. Andersen and Bejan [29] reported that the heat transfer rate through binary partitions is 20% less than the single partitions located in the middle of the cavity. Nakamura et al. [30] performed computational and experimental investigations in a chamber where the partition is vertically located in the center of the enclosure. Ho and Yih [31] adopted a numerical approach an studied the conjugated natural convection heat transfer inside a single partition cavity for different aspect ratios.

Effect of partitions on buoyancy induced convection and radiation inside cubic cavities have been considered by Parmananda et al. [32]. Different sources of irreversibilities were analyzed, and the importance of partitioning walls on entropy generation was noted. Considering the simultaneous effects of radiative-convective heat transfer, these authors suggested a practical choice in the design of buildings.

In the present work, the effect of various variables such as the inclination angle of the walls on natural convection the heat transfer inside a portioned trapezoidal cavity is theoretically investigated. A flexible divider partitions the trapezoidal enclosure into two sections, which could be applied to many practical applications, as mentioned. The streamlines and isotherms were presented for different values of Prandtl number, Rayleigh number, and inclination angle of vertical wall. Besides, the effect of Prandtl and Rayleigh number, on the maximum stress and flexible partition shape are discussed in detail.

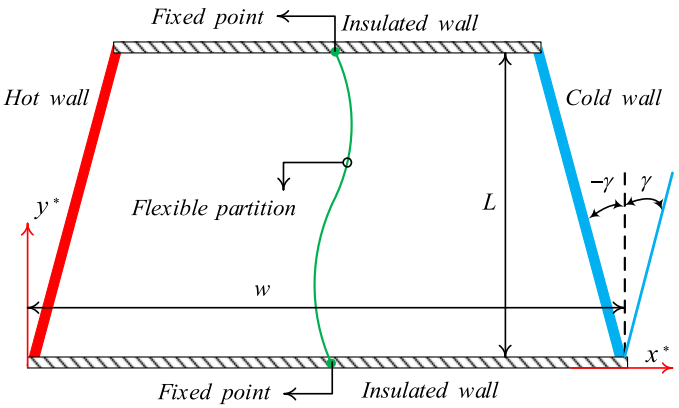

Fig. 1. Schematic view of the trapezoidal enclosure with the flexible partition.

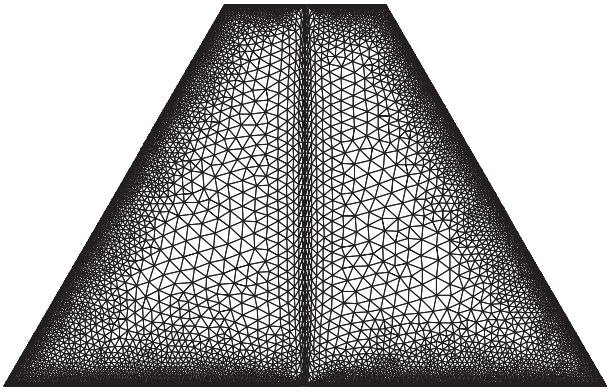

Fig. 2. A view of utilized grid.

2. Mathematical modeling

Considerable geometry of the current problem is depicted schematically in Fig. 1. The heat source associated with the hot bound imposes a high constant temperature T_h^* while the opposite cold one has a uniform temperature T_c^*. The horizontal bounds of the trapezoidal enclosure are thermally insulated. A thin and flexible separator is utilized to partition the trapezoidal enclosure into two smaller ones. The partition thickness is t_p^*. The partition is considered isotropic and there is no energy storage and temperature gradient in it since the partition is thin enough and acts as a high thermal conductive material. The fluid filling the enclosure behaves as an incompressible and Newtonian one. The present buoyancy-driven flow applies the Boussinesq approximation. This approximation neglects the variations of density except where they are in terms containing the gravity acceleration.

2.1. Fluid-Structure interaction (FSI) model

The reciprocal impacts of the flexible partition and fluid are modeled using the technique of the Arbitrary Lagrangian–Eulerian (ALE). Applying the ALE technique and above described assumes,

the governing equations are [33,34]:

$$\nabla^* \cdot \boldsymbol{u}^* = 0 \tag{1}$$

$$\frac{\partial \boldsymbol{u}^*}{\partial t} + (\boldsymbol{u}^* - \boldsymbol{w}^*) \cdot \nabla^* \boldsymbol{u}^* = -\frac{1}{\rho_f}\nabla^* P^* + \nu_f \nabla^{*2}\boldsymbol{u}^* + \beta_f \boldsymbol{g}(T^* - T_c{}^*) \tag{2}$$

Also, the energy equation which describes the temperature field can be represented as follows [34]:

$$\frac{\partial T^*}{\partial t} + (\boldsymbol{u}^* - \boldsymbol{w}^*) \cdot \nabla^* T^* = \alpha_f \nabla^{*2} T^* \tag{3}$$

The structural deformation of the separator is modeled through the following dynamic equation [33]:

$$\rho_s \frac{d^2 \boldsymbol{d}_s{}^*}{dt^2} - \nabla^* \boldsymbol{\sigma}^* = \boldsymbol{F}_v{}^* \tag{4}$$

In this study, the Neo-Hookean solid model has been employed for assigning the stress tensor σ^* [35]. The stress tensor, i.e., σ^*, is [14]:

$$\begin{array}{l} \boldsymbol{\sigma}^* = J^{-1} F S F^{tr} \\ F = (I + \nabla^* \boldsymbol{d}_s^*), J = det(F) \& S = \partial W_s / \partial \varepsilon \\ W_s = \frac{1}{2}\mu_l\left(J^{-1} I_1 - 3\right) - \mu_l \ln(J) + \frac{1}{2}\lambda(\ln(J))^2 \\ \varepsilon = \frac{1}{2}\left(\nabla^* \boldsymbol{d}_s^* + \nabla^* \boldsymbol{d}_s^{*tr} + \nabla^* \boldsymbol{d}_s^{*tr} \nabla^* \boldsymbol{d}_s^*\right) \\ \mu_l = E/2(1+\nu) \\ \lambda = E\nu/(1+\nu)(1-2\nu) \end{array} \tag{5}$$

2.2. Boundary and initial conditions

The mathematical forms of the boundary conditions are:

$$\begin{array}{l} u^* = v^* = 0,\ \partial T^*/\partial y^* = 0\ for\ upper\ and\ lower\ bounds \\ u^* = v^* = 0,\ T^* = T_h^*\ for\ left\ bound \\ u^* = v^* = 0,\ T^* = T_c^*\ for\ right\ bound \\ \frac{\partial \boldsymbol{d}_s^*}{\partial t} = \boldsymbol{u}^* \,\&\, \boldsymbol{\sigma}^* \cdot n_i^* = \left[-P^* I + \mu_f \nabla^* \boldsymbol{u}^*\right] \cdot n_i^*\ for\ flexible\ partiotion \\ \frac{\partial T^{*+}}{\partial n_i^*} = \frac{\partial T^{*-}}{\partial n_i^*}\ for\ left\ and\ right\ surfaces\ of\ partiotion \end{array} \tag{6-a}$$

n_i^* of the above relations is the perpendicular vector to the surface of the flexible partition. The mathematical form of the initial condition can also be written as follows:

$$u^* = v^* = 0,\ \begin{cases} T^* = T_h^*\ for\ the\ left\ sub-domain \\ T^* = T_c^*\ for\ the\ right\ sub-domain \\ T^* = \left(T_c^* + T_h^*\right)/2\ for\ the\ flexible\ partition \end{cases} \tag{6-b}$$

2.3. The no dimensional form of governing equations

Using the following non-dimensional parameters,

$$\begin{array}{l} \boldsymbol{d}_s = \frac{\boldsymbol{d}_s^*}{L}, \boldsymbol{\sigma} = \frac{\boldsymbol{\sigma}^*}{E}, \tau = \frac{t\alpha_f}{L^2}, (x, y, n_i) = \frac{(x^*, y^*, n_i^*)}{L} \\ \boldsymbol{u} = \frac{\boldsymbol{u}^* L}{\alpha_f}, \boldsymbol{w} = \frac{\boldsymbol{w}^* L}{\alpha_f}, P = \frac{L^2}{\rho_f \alpha_f^2}, T = \frac{T^* - T_c^*}{T_h^* - T_c^*} \\ \nabla = \frac{\nabla^*}{1/L}, \nabla^2 = \frac{\nabla^{*2}}{1/L^2}, t_p = \frac{t_p^*}{L} \end{array} \tag{7}$$

The governing equations describing the thermal and hydrodynamic behaviors of the fluid are:

$$\nabla \cdot \boldsymbol{u} = 0 \tag{8}$$

$$\frac{\partial \boldsymbol{u}}{\partial \tau} + (\boldsymbol{u} - \boldsymbol{w}) \cdot \nabla \boldsymbol{u} = -\nabla P + Pr \nabla^2 \boldsymbol{u} + Pr \boldsymbol{Ra} T \tag{9}$$

$$\frac{\partial T}{\partial \tau} + (\boldsymbol{u} - \boldsymbol{w}) \cdot \nabla T = \nabla^2 T \tag{10}$$

where

$$\boldsymbol{Ra} = \frac{\boldsymbol{g}\beta\left(T_h^* - T_c^*\right)L^3}{\upsilon_f \alpha_f}, Pr = \frac{\upsilon_f}{\alpha_f} \tag{11}$$

Also, the motion equation of the flexible partition is:

$$\frac{1}{\rho_R}\frac{d^2 \boldsymbol{d}_s}{d\tau^2} - E_\tau \nabla \boldsymbol{\sigma} = E_\tau \boldsymbol{F}_v \tag{12}$$

which

$$E_\tau = \frac{EL^2}{\rho_f \alpha_f^2}, \boldsymbol{F}_v = \frac{\left(\rho_f - \rho_s\right)L\boldsymbol{g}}{E}, \rho_R = \frac{\rho_f}{\rho_s} \tag{13}$$

The vector of $\boldsymbol{Ra}$ acts in the direction of the y-axis, upwards (gravity in downward direction). Since the Rayleigh number includes the vector of gravity acceleration, it has been represented as a vector. Indeed, the Rayleigh numbers in the x and y directions are respectively zero and $Ra = |\boldsymbol{Ra}|$. Here, E_τ is the non-dimensional Young's modulus. In this investigation, it is considered that $\rho_f = \rho_s$, hence, $\boldsymbol{F}_v = 0$ and $\rho_R = 1$. Applying the non-dimensional parameters defined in Eq. (7) to Eq. (6) yields to the non-dimensional boundary conditions:

$$\begin{array}{l} u = v = 0,\ \partial T/\partial y = 0\ for\ upper\ and\ lower\ bounds \\ u = v = 0,\ T = 1\ for\ left\ bound \\ u = v = 0,\ T = 0\ for\ right\ bound \\ \frac{\partial \boldsymbol{d}_s}{\partial \tau} = \boldsymbol{u},\ E_\tau \boldsymbol{\sigma} \cdot n_i = [-P + Pr\nabla \boldsymbol{u}] \cdot n_i\ for\ flexible\ partiotion \\ \frac{\partial T^+}{\partial n_i} = \frac{\partial T^-}{\partial n_i},\ T^+ = T^-\ for\ left\ and\ right\ surfaces\ of\ partiotion \end{array} \tag{14-a}$$

n_i of the above relations denotes the perpendicular vector to the surface of the partition in non-dimensionless coordinate. The initial condition imposed on the governing equations in non-dimensional space is:

$$u = v = 0,\ \begin{cases} T = 1 & for\ the\ left\ sub-domain \\ T = 0 & for\ the\ right\ sub-domain \\ T = 0.5 & for\ the\ flexible\ partition \end{cases} \tag{14-b}$$

Here, two definitions are expressed to evaluate the rate of heat transfer: first, the local Nusselt number along the left-side wall at a specified time is

$$Nu_l = \left.\frac{\partial T}{\partial n}\right|_{hot\ wall} \tag{15}$$

and then, the average Nusselt number for the hot wall at a specific time is defined as:

$$Nu_{av} = \cos\gamma \int_0^{1/\cos\gamma} Nu_l ds \tag{16}$$

where ds is the small element length along the left wall. Also, the dimensionless mean temperature in the whole enclosure is calculated as follows:

$$T_{av} = \frac{\int_A T_{local} dA}{\int_A dA} \tag{17}$$

Here, A denotes the domain of the enclosure. To describe the fluid flow inside the sub-cavities the concept of the stream function can be used as follows:

$$\nabla^2 \psi = -\nabla \times \boldsymbol{u} \tag{18}$$

3. The numerical method, grid independence test, and validations

The interdependent, complex and non-linear Eqs. (8–10) and (12) are solved by employing the Galerkin finite element method

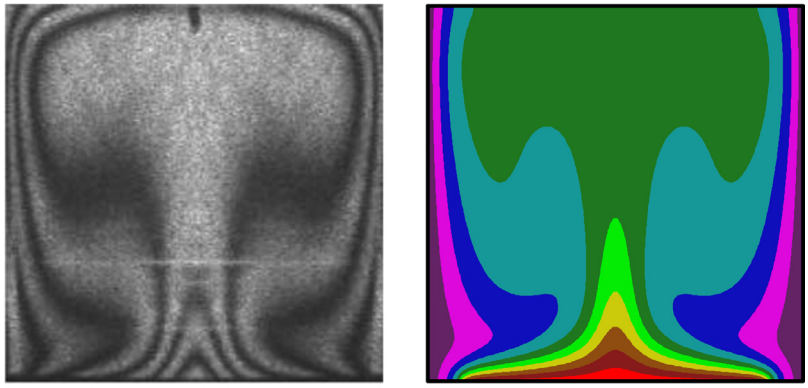

a b

Fig. 3. Comparison between the temperature field obtained by Calcagni et al. [38] and the results of the present study; (a) Calcagni et al. [38] and (b): temperature field of the current investigation.

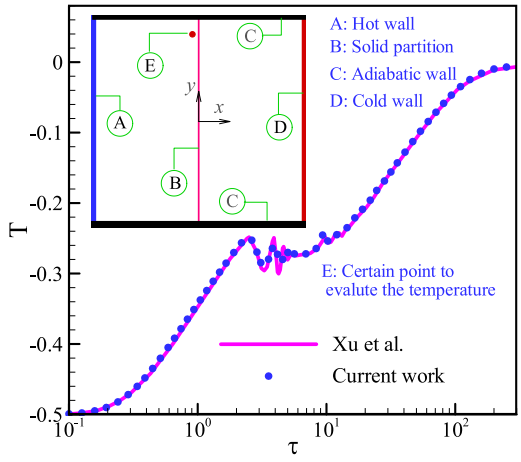

Fig. 4. The temperature of the indicated point in the cavity of the current investigation and work of Xu et al. [39].

Table 1
Grid independency results for Ra = 10^7 and Pr = 6.2, $E_\tau = 5 \times 10^{11}$ and $\gamma = -30°$

Case number (i)	1	2	3	**4**	5
Number of elements	10,529	13,939	18,397	**25,088**	37,237
Nu_{av}	7.2245	7.3864	7.3993	**7.4045**	7.4047
*Error (%)	–	2.2409	0.1746	**0.0702**	0.0027

*Error(%) = $(Nu_{av,i+1} - Nu_{av,i}) \times 100/Nu_{av,i}$

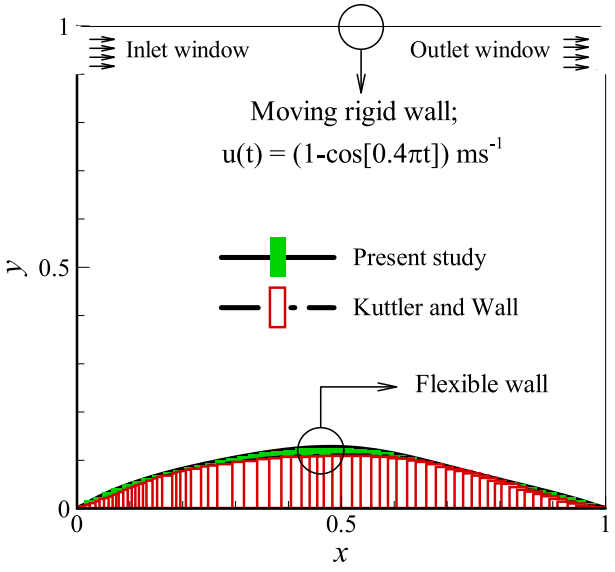

Fig. 5. Displacement of the flexible wall of the current study and the work of Kuttler and Wall [40].

(FEM) with the aid of Arbitrary Lagrangian–Eulerian (ALE) technique. Some aspect of the numerical approach of the finite element is expressed in [36,37]. In this work, the Gaussian quadrature based on the finite element method (FEM) provides smooth solutions at the internal sub-domains. A mesh made of non-uniform triangular elements is employed to discretize the studied domain. Before providing the results, of necessity is to get grid-independent results and to verify their correctness. Thus, several cases applying different grid sizes are tested to capture grid-independent results. As tabulated in Table 1, a grid with 25,088 elements can minimize the impacts of the grid on the accuracy of the results.

To guarantee the correctness of the numerical outcomes, the utilized solver is validated in three steps. Firstly, as illustrated in Fig. 3, the natural convection flow in an enclosure occupied with air is simulated well, as per comparison with the temperature filed given by Calcagni et al. [38]. Secondly, the transient simulation is validated through the local temperature at a certain point presented at the work of Xu et al. [39], as depicted in Fig. 4. In the work of Xu et al. [39], an square enclosure was divided into two sub-domains by a solid conductive partition. The left and right sidewalls of the enclosure were isothermally kept at low and high temperatures. While the horizontal walls were considered to be adiabatic. At $t = 0$, water as the working fluid on the left side of the partition was cold, and that on the other side of the partition was hot. The values of non-dimensional parameters in this work were Ra=9.2 × 10^8, and Pr=6.63. The designated point to extract the local temperature over time is located at (−0.0083,0.375). As exhibited in Fig. 4, the local temperature at the designated point exhibits a good agreement with the results presented by Xu et al. [39]. Finally, displacement of the flexible wall of a cavity is simulated and compared with the results of Kuttler and Wall [40]. As demonstrated in Fig. 5, the utilized solver is confirmed to have good potency for simulating the displacement of flexible partition.

4. Results and discussion

This part presents the outcomes acquired from the numerical simulation. The effects of the different non-dimensional pa-

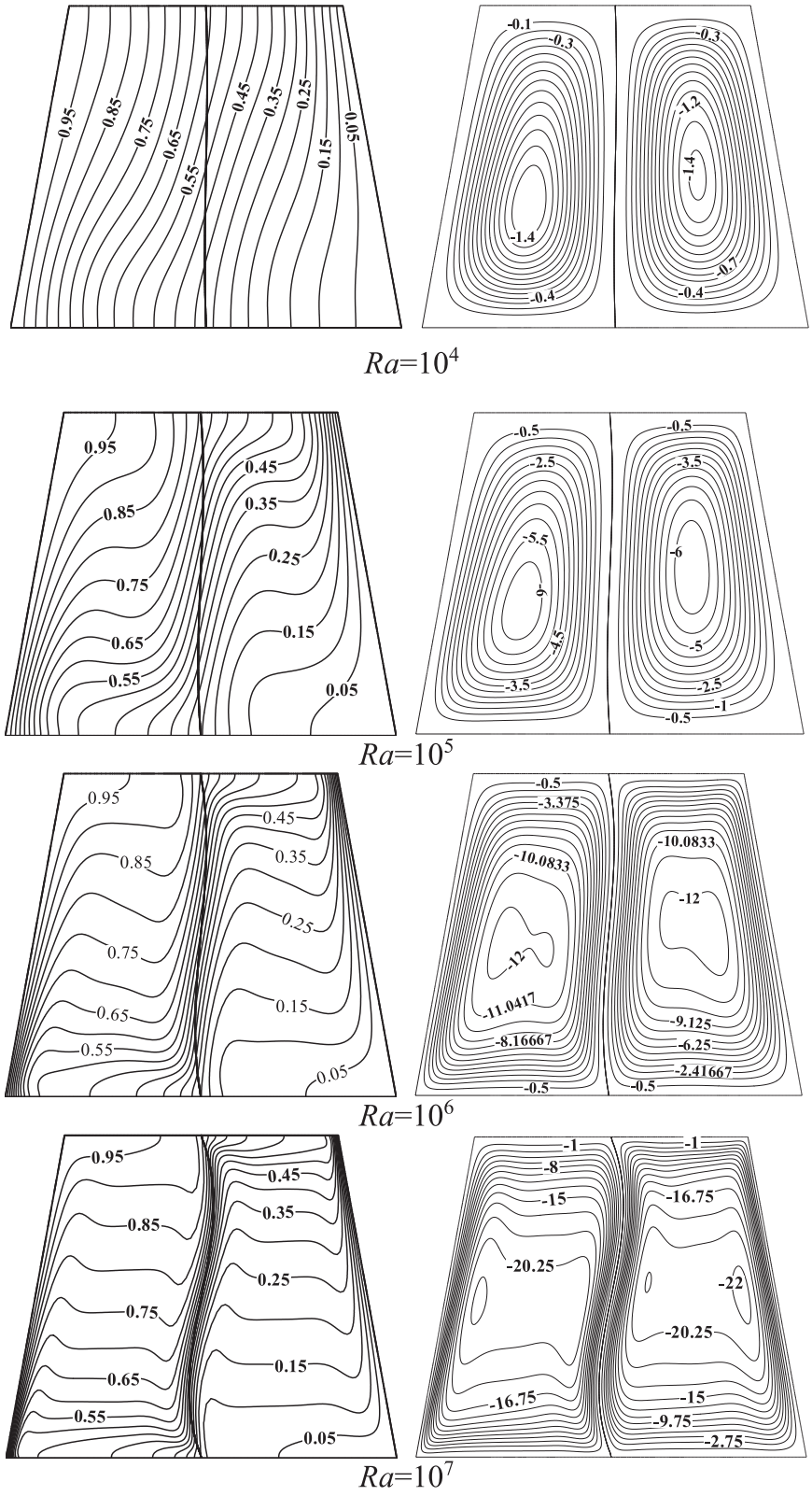

Fig. 6. Effect of Rayleigh number on Streamlines (left) and isotherm (right) at steady state when Pr = 6.2, $E_\tau = 5 \times 10^{12}$ and $\gamma = -10°$.

rameters such as Rayleigh number ($10^4 \le Ra \le 10^7$), the inclination angle of the cavity sidewalls ($-30° \le \gamma \le 30°$), Hartmann number ($10^{10} \le E_\tau \le 10^{13}$) and the Prandtl number ($0.7 \le Pr \le 200$) on the streamlines and isotherms contours in the cavity are studied. Furthermore, the study of impacts of mentioned parameters on the stress of the partition and its deflection is conducted. As previously mentioned, ρ_R and $\boldsymbol{F}_v$ always have the values of 1 and 0.

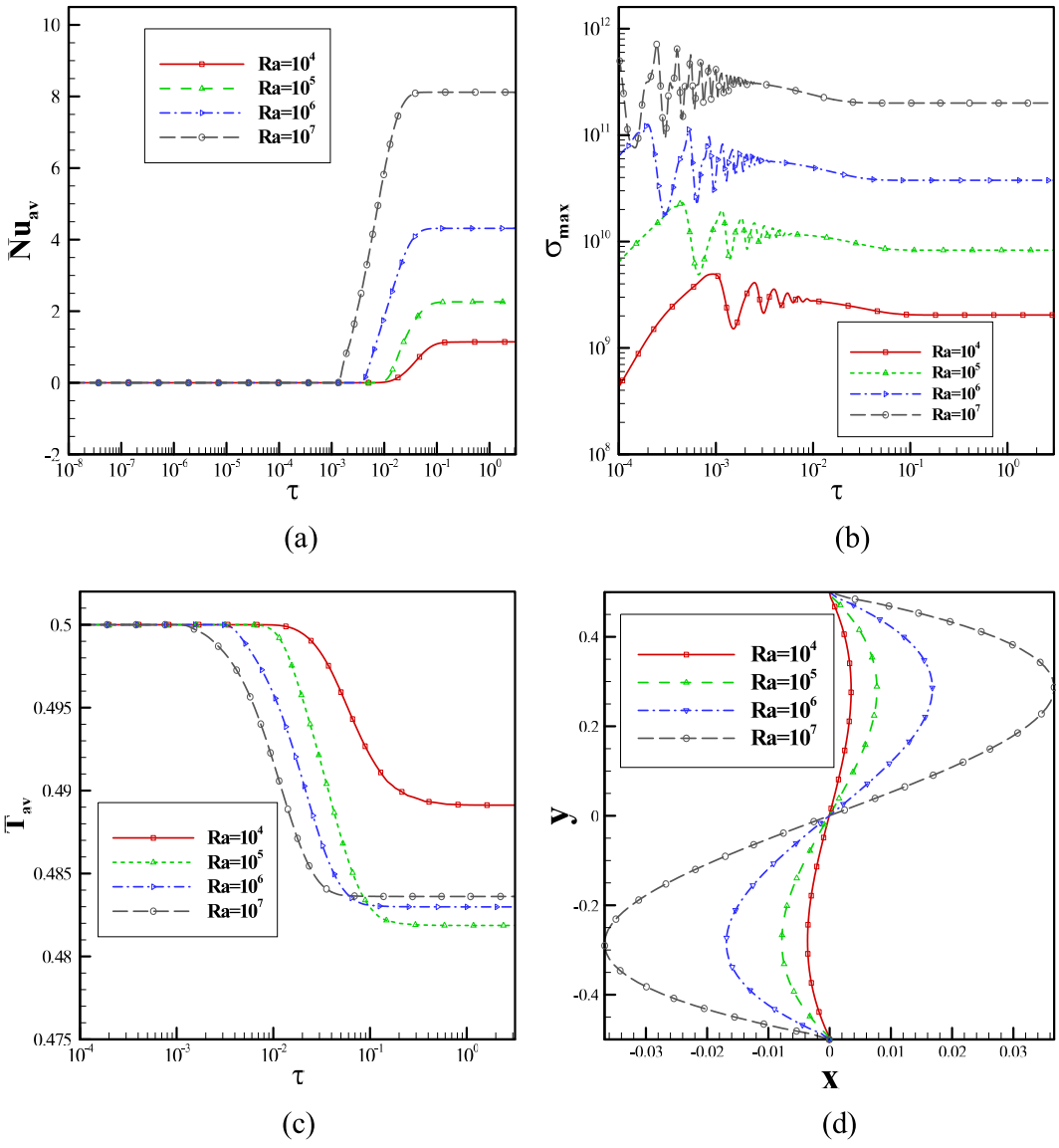

Fig. 7. Effect of Rayleigh number as a function of non-dimensional time (τ) when Pr = 6.2, $E_\tau = 5 \times 10^{12}$, and $\gamma = -10°$; (a): average heat transfer rate (Nu_{av}), (b): maximum tensions of partition (σ_{max}), (c) average temperature of the enclosure (T_{av}), and (d): the steady-state deformed shape of the partition.

4.1. Rayleigh effect

Rayleigh number *Ra* is varied between 10^4 and 10^7. The Prandtl number is fixed at 6.2, which is the Prandtl number of water, the angle of trapezoidal is $-10°$, and the elasticity modulus in non-dimensional form is 5×10^{12}.

The streamlines and the isothermal contours in the cavity for different values of Rayleigh numbers *Ra* are depicted in Fig. 6. For $Ra = 10^4$ and $Ra = 10^5$, the streamlines present a similar behavior in the left and right portions of the cavity. A single circulation zone is present in each portion, and the flexible membrane remains almost vertical. As *Ra* is increased to 10^5, the central vortex inside the circulation zone elongates and starts to divide into two vortices. The complete division is achieved for $Ra = 10^6$, where two vortices appear in the center of the circulation. The distribution of the streamlines is denser near the walls and the flexible membrane, indicating a more intense flow in those regions. Moreover, the flexible membrane is deformed to the left due to the solid-structure interaction force. In fact, *Ra* is an indicator of the relative importance between the buoyancy forces and the viscous forces. When *Ra* is increased, buoyancy dominates the resistive viscosity and the flow is intensified. Conversely, at low *Ra*, the flow intensity is low, and the pressure is almost the same in the two portions of the cavity, and as a result, the flexible membrane does not deform.

Looking at the isothermal contours in Fig. 6 shows that the isotherms shift from being almost vertical at low *Ra* to being horizontal when *Ra* is increased. This indicates that the mechanism of heat transfer changes with the variation of *Ra* for low *Ra*, the heat transfer is dominated by conduction. As *Ra* increases, the rise of the buoyancy effects leads to a stratification of the isotherms pattern due to stronger convective currents, while simultaneously, conduction is inhibited. Therefore, increasing *Ra* changes the heat transfer mode from being conduction-dominated mode to convection-dominated. The onset of this shift in the heat transfer mode can be set for *Ra* between 10^5 and10^6, where the isotherms begin to become horizontal, and the membrane starts to deform.

The effect of *Ra* on the variation of the average Nusselt number at the hot wall Nu_{av} as a function of time is shown in Fig. 7(a). At initial times, the sub-cavity next to the cold wall is at an initial

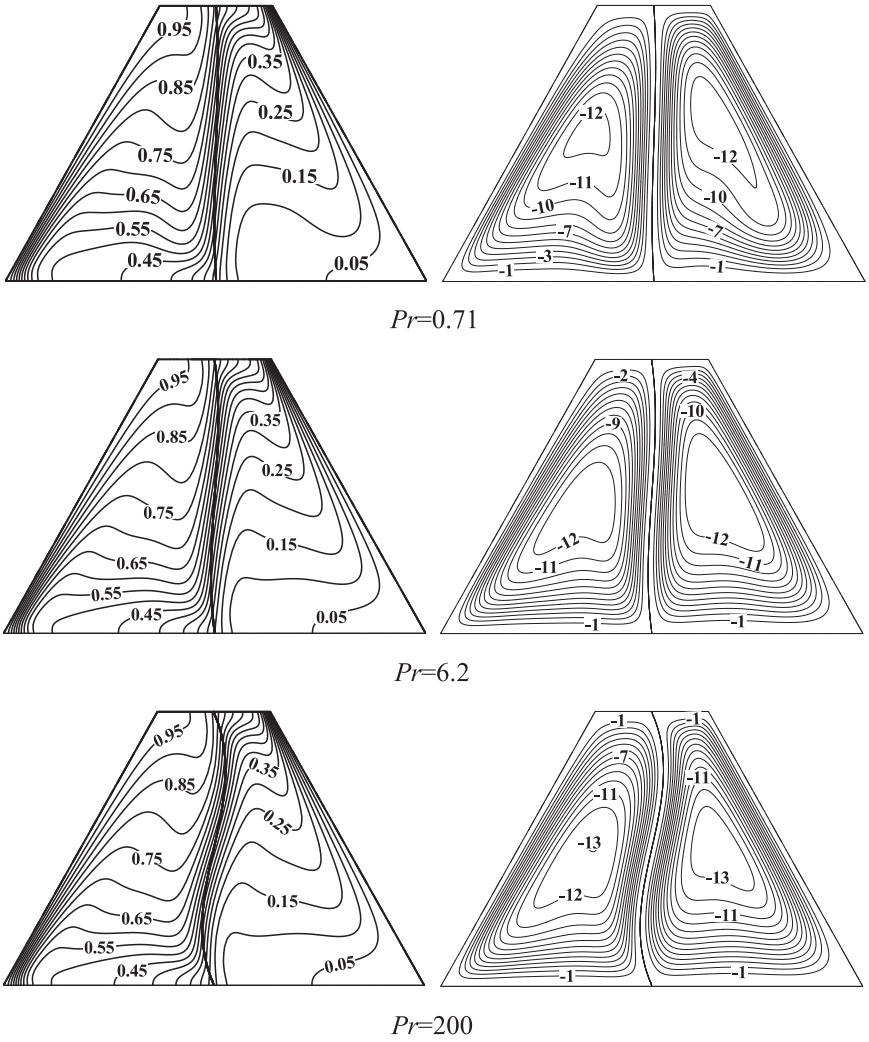

Fig. 8. Effect of Prandtl number on the steady-state streamline (left) and isotherm (right) when Ra=106, E_τ=1013, and $\gamma=-30°$.

cold temperature while the sub-cavity next to the hot wall is at an initial hot temperature. In this situation, the isotherm walls are at the same temperature as the fluid next to the wall. Hence, there is no initial heat transfer. After a while, the temperature distribution in the cavity changes, and the heat transfer from the hot to cold commence. As the fluid starts to circulate, free convection takes place, and Nu_{av} increases. It is clear that steady Nu_{av} rises with the increase of *Ra*. This is due to the fact that convective transfer is enhanced when the buoyancy effects in the flow are more significant, i.e., when *Ra* is increased. As a result, the overall heat transfer is improved and Nu_{av} increases. An 800% rise in the value of Nu_{av} can be achieved when *Ra* is increased from 10^4 to 10^7.

Fig. 7(b) shows the variation of the maximum stress σ_{max} in the membrane as a function of time for different values of *Ra*. It is shown that a higher value of σ_{max} is obtained when *Ra* is increased. This result is in accordance with the observations of Fig. 6. As *Ra* is increased, the flow is intensified, raising the magnitude of the fluid-structure forces affecting the membrane. This leads to deflecting the membrane and to correspondingly increasing the value of σ_{max}.

Fig. 7(d) depicts the shape of the flexible partition for different values of *Ra*. It is shown that more deformation is obtained for higher *Ra*. This result is closely related to Fig. 7(c). As discussed earlier, the enhancement of buoyancy force in the cavity due to the increase of *Ra* enhances the fluid-structure forces, which deform the flexible membrane. It can also be seen that the deflection of the membrane is symmetrical around the vertical middle ($x = 0$) of the cavity. This is due to the symmetry of the cavity and the location of the membrane in the middle. The rise of the buoyancy forces for a higher *Ra* enhances the convective flow where the hot fluid goes to the top and exerts more interaction forces. This is apparent in the left hot portion of the cavity, where the membrane is deflected to the right. On the other side, the cold fluid goes down, manifestly in the right cold portion, and exerts forces in the opposite direction. This opposite circulation between the rising hot fluid and the descending cold fluid leads to a double effect on the flexible partition which, consequently, deforms into an S-shape.

The effect of *Ra* on the variation of the mean temperature in the enclosure T_{av} as a function of time is illustrated in Fig. 7(c). Initially, the average temperature in the cavity is equal to T_{av}=0.5, i.e. the mean value between the cold and hot walls. This remains the case when heat transfer is near the boundaries and dominated by conduction. As convection starts to occur, heat is transferred from the hot to the cold wall and the cavity cools down. As a consequence, T_{av} decreases. It is shown that T_{av} is at its highest for $Ra = 10^4$, which can be related to the inhibited heat transfer in that case as discussed in Fig. 7(a). However, when *Ra* is increased, T_{av} presents a minimum for $Ra = 10^5$ and increases with the rise of *Ra*. This indicates that despite the enhancement of the heat transfer due to the increase of *Ra*, the presence of the membrane affects

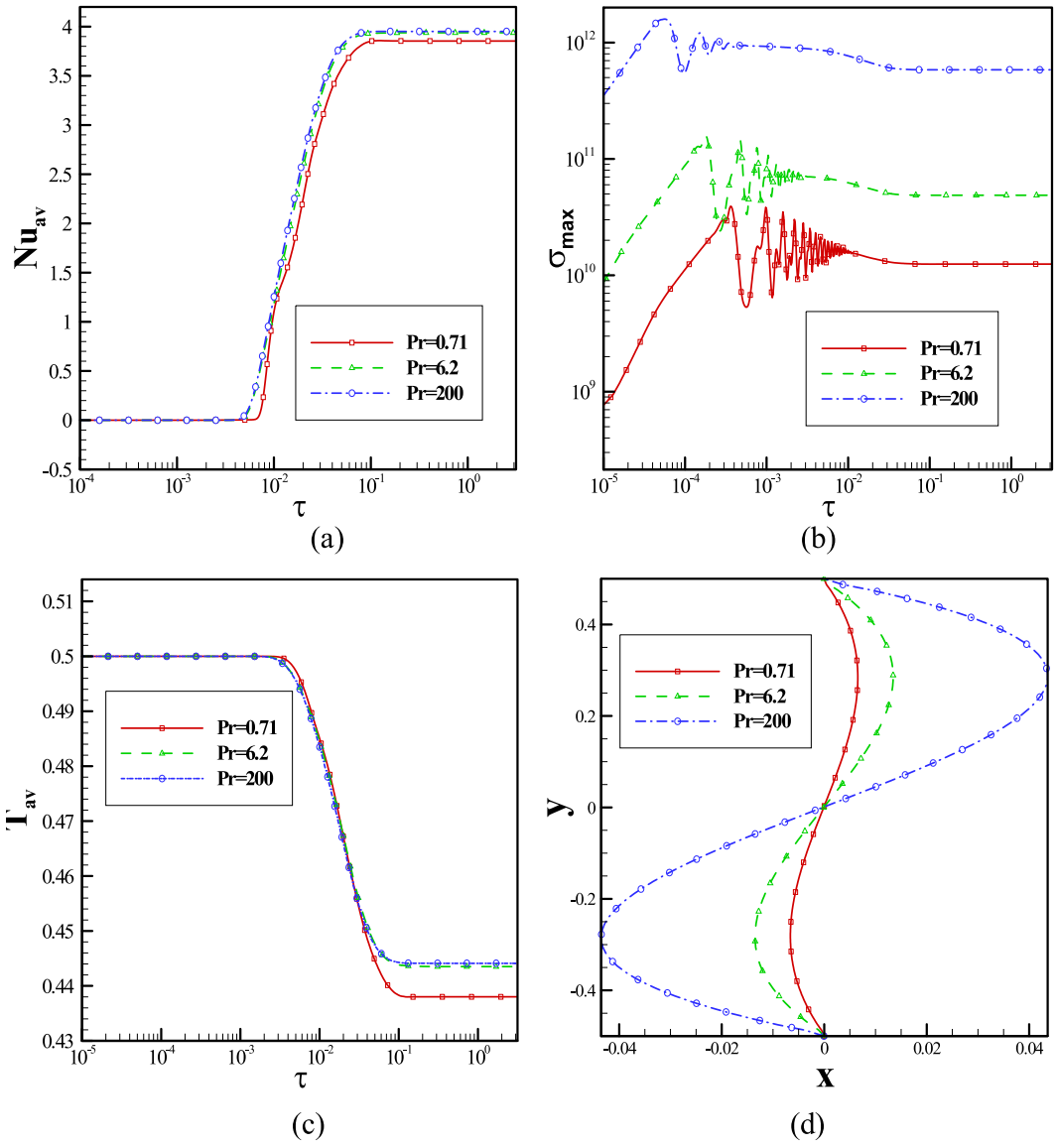

Fig. 9. Effect of Prandtl number as a function of non-dimensional time (τ) when Ra = 10^6, E_τ = 10^{13}, $\gamma = -30°$; (a): average heat transfer rate (Nu_{av}), (b): maximum tensions of partition (σ_{max}), (c) average temperature of the enclosure (T_{av}), and (d): steady-state deformed shape of the partition.

the thermal distribution and gives rise to a higher average temperature in the cavity. It can thus be concluded that no outright relation between T_{av} and Ra can be inferred due to the disturbance of the thermal patterns caused by the membrane.

4.2. Prandtl number effect

In this section, the effect of Prandtl number Pr on Nu_{av}, T_{av}, and σ_{max} is evaluated. The values used for Pr are 0.71, 6.2, and 200, which correspond respectively to air, water, and engine oil as working fluids. Rayleigh Number is 10^6, the elasticity modulus in non-dimensional form is $10^{13,}$ and γ is fixed at $-30°$

Fig. 8 shows the steady streamlines and isothermal contours for different values of the Prandtl number Pr. It is shown that increasing Pr has a slight effect on the streamlines profile, but it leads to denser streamlines indicating a more intense fluid flow. In addition, while the flexible membrane remains vertical in the case of air as working fluid ($Pr = 0.71$), it presents a symmetric deformation when engine oil is used ($Pr = 200$). In fact, Pr represents the relative importance of momentum diffusion with respect to heat diffusion. A rise in the momentum diffusion when Pr is increased leads to an intensified flow. The distribution of the isotherms follows the flow patterns, where the volume of the hot and cold portions of the cavity changes due to the deformation of the flexible membrane located in the middle, which occurs for higher Pr.

Fig. 9(a) illustrates the effect of Pr on the variation of Nu_{av} as a function of time. It can be seen that increasing Pr enhances heat transfer by increasing Nu_{av} in the steady-state flow. For low Pr, the thermal diffusivity overcomes momentum diffusivity and conduction dominates heat transfer. As Pr is increased, momentum diffusivity dominates, and convection plays a more effective role in energy transfer inside the cavity. Using engine oil ($Pr = 200$) as a working fluid instead of air ($Pr = 0.71$) increases the value of Nu_{av} by 4%, which cannot be considered very significant. It can be also noted that water and engine oil ($Pr = 6.2$ and $Pr = 200$) present the same value of Nu_{av}. In fact, these two values of Pr can both be considered substantially greater than 1. In both situations, the increased impact of convective effects due to the rise in the momentum diffusion is similar. Therefore, increasing Pr, when it is already higher than a critical value greater than 1, does not affect heat transfer inside the cavity.

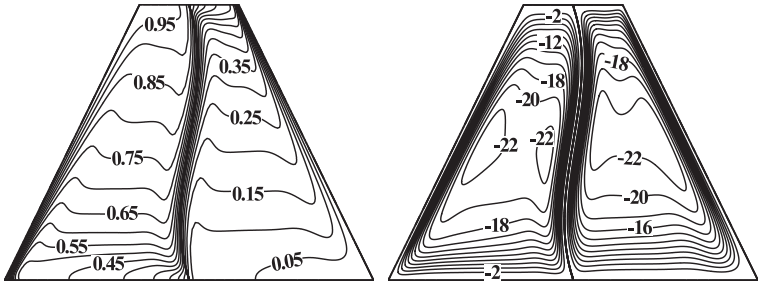

γ=-30°

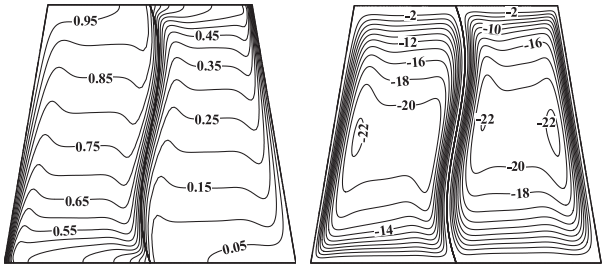

γ=-10°

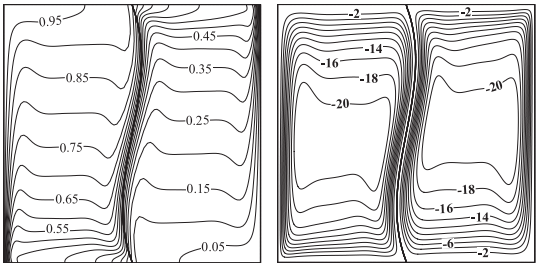

γ=0°

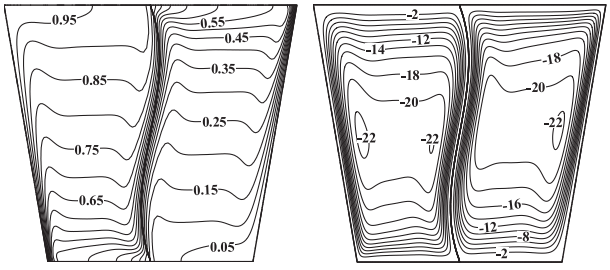

γ=+10°

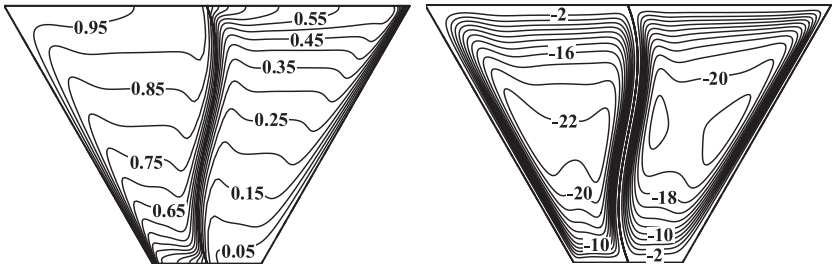

γ=+30°

Fig. 10. Effect of γ on the steady-state streamline (left) and isotherm (right) when Ra = 10^7, E_τ = 10^{13}, and Pr = 6.2.

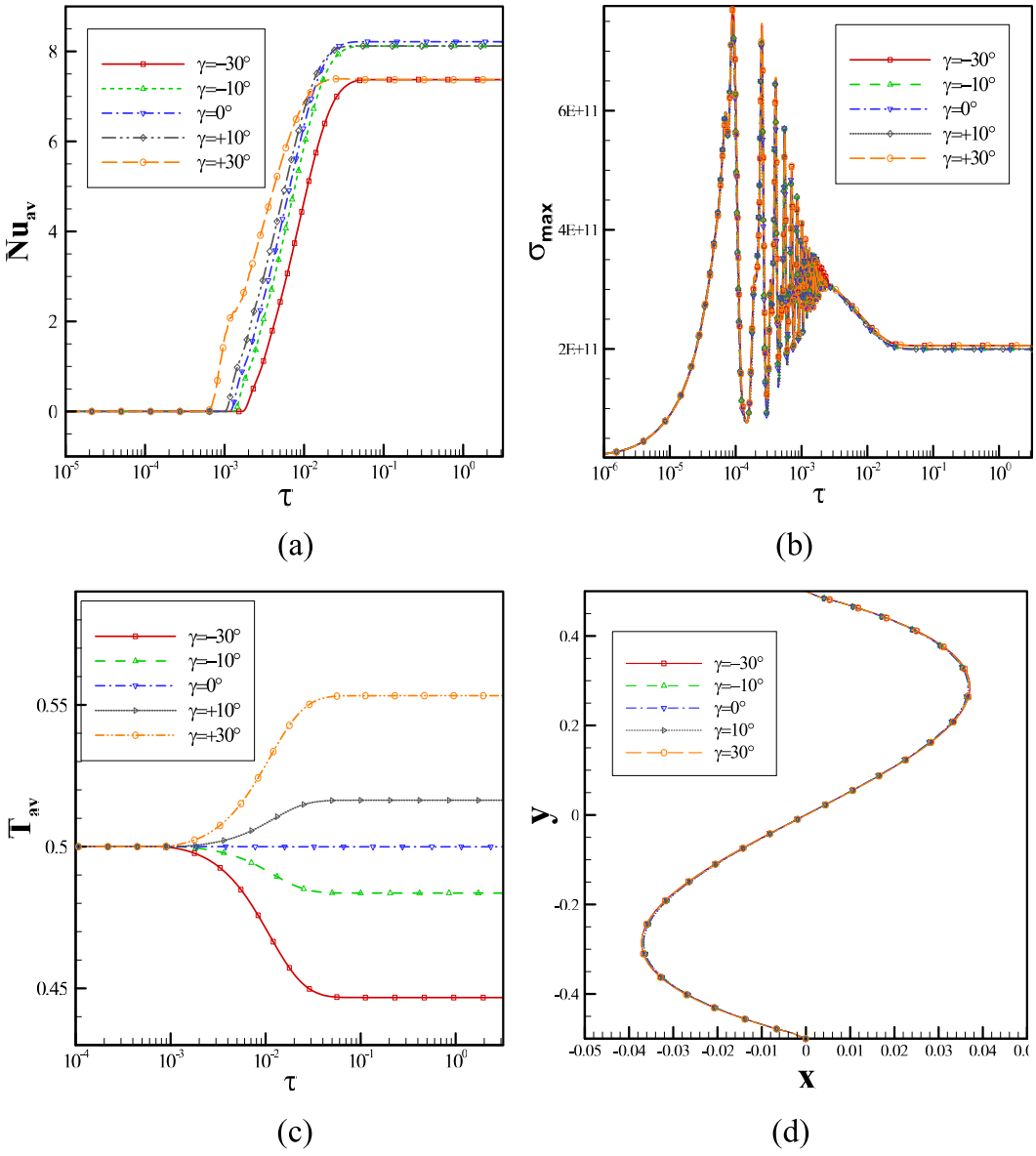

Fig. 11. Effect of walls inclination angle (γ) as a function of non-dimensional time (τ) when Ra = 10^7, E_τ = 10^{13}, and Pr = 6.2; (a): average heat transfer rate (Nu_{av}), (b): maximum tensions of partition (σ_{max}), (c) average temperature of the enclosure (T_{av}), and (d): steady-state deformed shape of the partition.

The variation of σ_{max} as a function of time for different values of *Pr* is shown in Fig. 9(b). It is clear that σ_{max} rises when *Pr* is increased. As observed in Fig. 8, when *Pr* is increased, the flow is intensified in the cavity and, more particularly, near the flexible membrane. This intensification is due to the increased momentum diffusivity between the molecules of the fluid. As the flow intensifies, the fluid-structure forces amplify in magnitude and the maximum stress in the membrane increases. Raising *Pr* from 6.2 to 200 increases significantly the value of σ_{max}. Therefore, the effect of increasing *Pr* on fluid-structure interaction is important even if the initial value of *Pr* is substantially higher than 1, unlike was what observed for heat transfer in Fig. 9(a).

4.3. Walls inclination angles (γ) effect

Here, the effect of cavity wall inclination angles (γ) on Nu_{av}, T_{av} and σ_{max} is investigated. Rayleigh number *Ra* is adopted as 10^7, and Prandtl number is 6.2, which is water's Prandtl number, and elasticity modulus in non-dimensional form is 5×10^{12}. Changing γ gives insights about the effects of the inclination of the cavity sidewalls, as well as the locations of the larger and smaller bases of the trapezoidal cavity, on heat transfer and fluid flow.

Fig. 10 shows the steady-state streamlines and the isotherms for different values of the enclosure walls inclination angle γ. For the square enclosure ($\gamma = 0°$), circulation zones symmetrical around the membrane appear in the two portions of the cavity. When the side walls are tilted ($\gamma \neq 0°$), additional vortices appear in the center of the circulation zones due to the disturbance of the flow fields resulting from the walls inclination and the geometrical change of the surface in which the fluid is flowing. Comparing the streamline patterns in the cases $\gamma = +30°$ (larger base at the top) to $\gamma = -30°$ (smaller base at the top) shows that looking at one of these cases upside down leads to the same pattern of the other. The behavior obtained in the left portion of the cavity for $\gamma = +30°$ is similar to the one obtained in the right portion for $\gamma = -30°$ and vice versa. The same observation can be obtained by comparing the cases $\gamma = +10°$ and $\gamma = -10°$ Therefore, varying the inclination angle from a positive value to the opposite negative

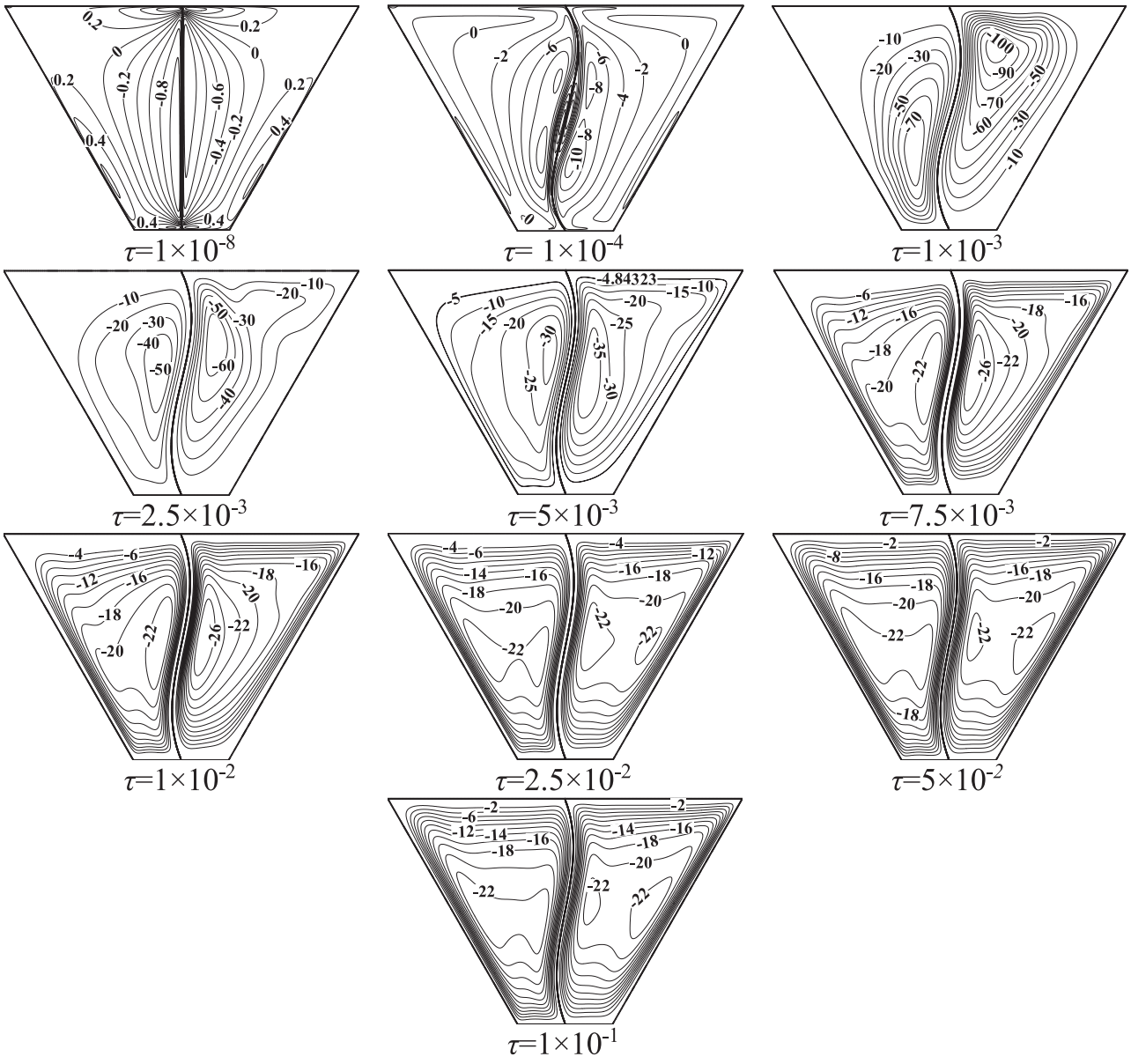

Fig. 12. Time variation of streamlines when Ra = 10^6, Pr = 6.2, $E_\tau = 5 \times 10^{12}$, and $\gamma = -30°$.

value, and therefore exchanging the locations of the smaller and larger bases, causes a change in the streamlines to pattern symmetrical around the vertical mid-line of the cavity.

It should also be noted that for all the values of γ, the flexible membrane shows similar deflection, to the right in the top region and to the left in the bottom. The isothermal contours are shown in Fig. 10 follow the fluid flow development in the two portions of the cavity. For instance, for $\gamma = +30°$, the isotherms 0.9 and 0.5 are long horizontal lines, while they are very short near the top for $\gamma = -30°$ As the hot fluid moves upward due to density change, the increased space near the top in the case $\gamma = +30°$ allows a greater zone of high temperature in that space, while the opposite happens in the case $\gamma = -30°$ A similar trend is observed for the cases $\gamma = +10°$ and $\gamma = -10°$ As for the case $\gamma = 0°$, most of the isotherms are represented by horizontal lines between the top and the bottom of the cavity, indicating a balanced distribution of the temperature between the hot and cold fluid flowing in the cavity.

The effect of γ on the heat transfer in the cavity is illustrated in Fig. 11(a). The steady value of Nu_{av} is at its highest for a square cavity ($\gamma = 0°$) is slightly lower in trapezoidal cavities when cavity walls are slightly tilted ($\gamma = \pm 10°$), and decreases by almost 11% when the side walls are more inclined ($\gamma = \pm 30°$), This indicates that the disturbance of the flow patterns induced by the inclination of the cavity sidewalls does not contribute positively to the convective heat transfer. As the flow patterns just change location between the left and right portions of the cavity when the larger base is moved from the top to the bottom or inversely (the sign of γ changed, but the same value was kept), the overall intensity of the flow remains the same and no further contribution to convection is obtained, which might explain why the same value of Nu_{av} is obtained in the cases $\gamma = +30°$ and $\gamma = -30°$ and the cases $\gamma = +10°$ and $\gamma = -10°$

The variation of σ_{max} as a function of time for different values of γ is plotted in Fig. 11(b). It is clear that in the steady-state, σ_{max} remains almost the same for all the values of the inclination angle. In fact, while the change in the flow patterns might change the distribution of the stresses on the membrane due to the change of the surfaces in which the fluid is flowing from the top to the

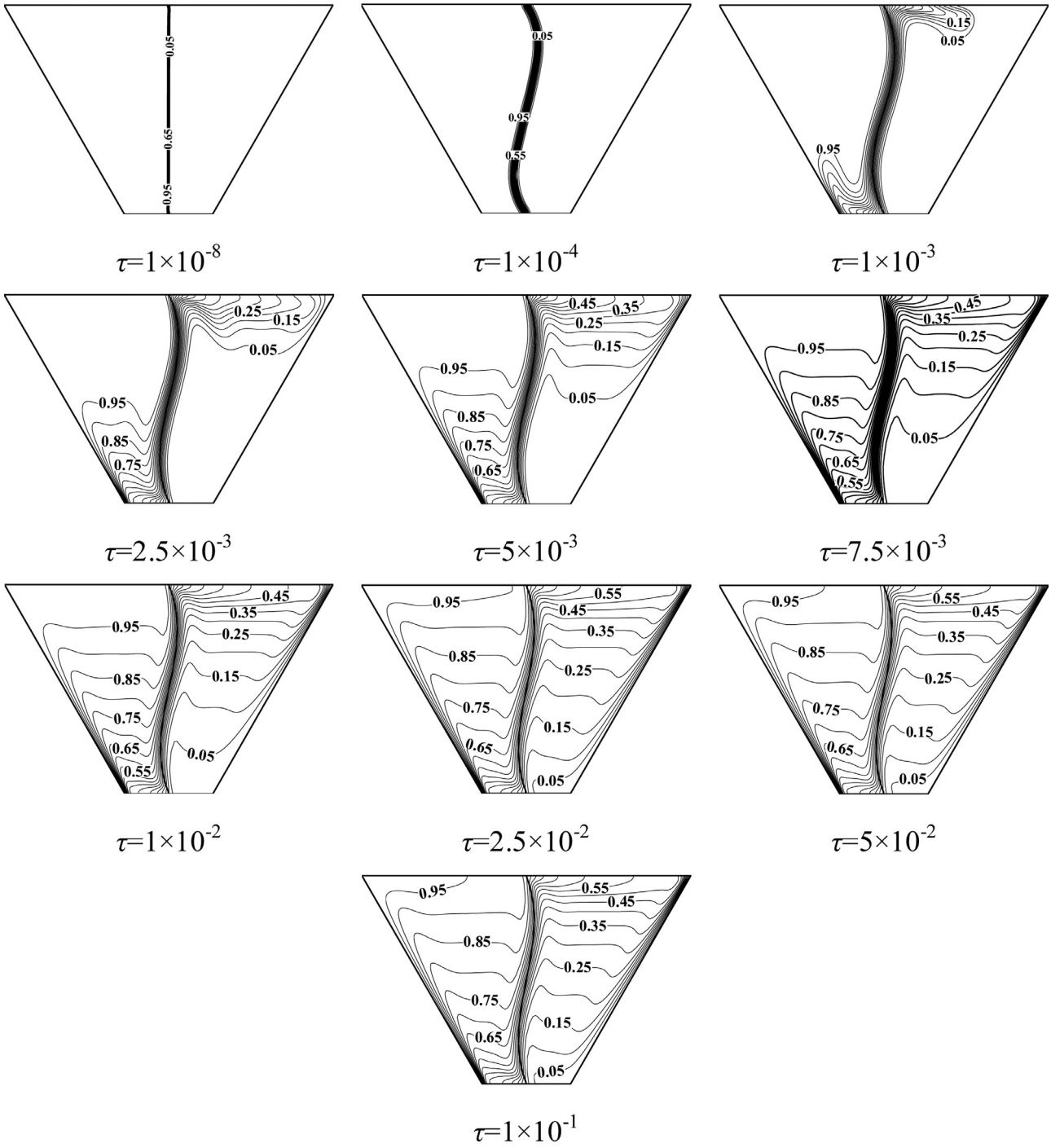

Fig. 13. Time variation of isotherms when Ra = 10^6, Pr = 6.2, $E_\tau = 5 \times 10^{12}$, and $\gamma = -30°$.

bottom, it does not affect the maximum stress in the membrane. For instance, when the larger base is at the top, while more fluid is flowing in the top, less flow is occurring near the bottom and the overall fluid-structure interaction forces are balanced and are similar to the forces that arise in a cavity with the larger base at the bottom. The maximum stress would then be almost the same for the different inclination angles of the side walls.

The variation of T_{av} as a function of time for different values of γ is shown in Fig. 11(c). It is shown that a higher T_{av} is obtained when the inclination angle is increased from $-30°$ to $+30°$ In fact, as discussed in Fig. 10 about the isotherm contours distribution, placing the larger base of the trapezoid at the top gives more space to the hot fluid moving upward and less space to the cold one going down in the two portions of the cavity, leading thus to the higher average temperature in the enclosure. For the s cavity ($\gamma = 0°$), T_{av} is equal to 0.5 due the symmetry of the geometry and the resulting balanced distribution between the hot and cold zones of the flow.

Fig. 11 (d) depicts the effect of γ on the shape of the flexible partition. It is obvious that the variation of the inclination angle of the side walls has a very limited effect on the deformation of the flexible membrane. This result is closely related to the observations discussed in Fig. 11(b). The membrane shows the same shape after deflection in all the cases due to the presence of fluid-structure

interaction forces of the same magnitude, as the inclination angle does not impact the overall intensity of the flow inside the cavity.

Figs. 12 and 13 illustrate the isothermal contours and the streamlines, respectively. The results are depicted for different time steps until reaching the steady-state condition. Initially ($\tau = 1 \times 10^{-4}$), the flexible membrane is vertical, and the fluid starts to flow around the membrane. Near the cavity sidewalls, flow streamlines develop near the bottom as the fluid is slowly moving upwards. Shortly after ($\tau = 1 \times 10^{-4}$), the membrane is deformed to its final position, and the fluid is flowing slowly in the entire cavity. As time goes, the flow accelerates, and at ($\tau = 7.5 \times 10^{-3}$) the streamlines are dense near the membrane, as it is preventing the fluid from moving from the left portion to the right one. As the flow keeps accelerating, vortices appear in the circulation zone of the fluid, with almost the same flow velocity distribution in the left and right portions of the cavity when the steady-state condition is achieved ($\tau = 1 \times 10^{-1}$).

The isothermal contours follow the evolution of the flow patterns in the two portions of the cavity. The hot fluid moves upwards, and the cold one moves in the opposite direction. The temperature in the left portion is between 0.4 and 1, while in the right portion, it remains limited between 0 and 0.7, due to the presence of the membrane, which limits the heat transfer between the portions. Moreover, the shape of the streamlines shows a shift in the heat transfer dominant mechanism from conduction in the first instants ($\tau = 1 \times 10^{-3}$) to convection in the steady-state ($\tau = 1 \times 10^{-1}$) when the flow is fully developed.

5. Conclusion

The flow, temperature and stress field for natural convection heat transfer in a trapezoidal enclosure with a flexible partition were investigated theoretically. The fluid-structure interaction approach, including a moving mesh technique, is applied to model the large deformations of the flexible partition. The finite element method was employed to solve the governing equations for the flow and temperature field in the cavity and partition, as well as, the tensions and displacements in the partition. Grid checks and validations are performed, and the results were found in agreement with the literature. The effect of various non-dimensional parameters on the thermal and mechanical behavior of the cavity was analyzed. The main outcomes of the study can be concluded as follows:

- Increasing Rayleigh number *Ra* enhances heat transfer in the cavity and leads to an increase in the maximum stress in the flexible membrane, which deforms consequently. This results from the dominance of buoyancy forces at high *Ra* which increases the fluid-structure interaction forces and enhances the convective heat transfer in the cavity.
- While raising Prandtl number *Pr* has a slight impact on heat transfer inside the cavity; it affects the fluid-structure interaction by increasing the maximum stress in the flexible membrane and its deformation. This is due to the increase in the momentum diffusivity in the fluid.
- The effect of the inclination angle of the sidewalls on the maximum stress and the deformation of the flexible partition is very limited. Heat transfer is maximum in a square cavity and decreases with the increase of the inclination degree of the cavity walls. The larger base of the cavity being at the top (positive inclination angle) or the bottom (negative inclination angle) has no effect on the heat transfer rate in the cavity. However, the average temperature in a cavity is higher when the larger base is at the top.

In the present study, the fluids in both sub-sections were similar, and the flexible partition was acting as a separator or a filtration media. This situation can be applied in fuel cells and chemical processes for fluids with a small variation in concentration. Hence, the effect of the static pressure was negligible. However, there are also applications, in which, the flexible partition acts as a membrane to separate two different fluids. In this case, the static pressure can play a significant role and can be subject to future studies.

Declaration of Competing Interests

The authors declare that they have no known competing financial interests or personal relationships that could have appeared to influence the work reported in this paper.

Supplementary materials

Supplementary material associated with this article can be found, in the online version, at doi:10.1016/j.ijheatmasstransfer.2019.119186.

References

[1] M. Ghalambaz, A. Noghrehabadi, A. Ghanbarzadeh, Natural convection of nanofluids over a convectively heated vertical plate embedded in a porous medium, Braz. J. Chem. Eng. 31 (2) (2014) 413–427.

[2] M. Ghalambaz, A. Behseresht, J. Behseresht, A. Chamkha, Effects of nanoparticles diameter and concentration on natural convection of the Al2O3–water nanofluids considering variable thermal conductivity around a vertical cone in porous media, Adv. Powder Technol. 26 (1) (2015) 224–235.

[3] M. Izadi, N.M. Maleki, I. Pop, S. Mehryan, Natural convection of a hybrid nanofluid subjected to non-uniform magnetic field within porous medium including circular heater, Int. J. Numer. Methods Heat Fluid Flow 29 (4) (2019) 1211–1231.

[4] M. Izadi, R. Mohebbi, A. Chamkha, I. Pop, Effects of cavity and heat source aspect ratios on natural convection of a nanofluid in a C-shaped cavity using lattice Boltzmann method, Int. J. Numer. Methods Heat Fluid Flow 28 (8) (2018) 1930–1955.

[5] S. Mehryan, M. Ghalambaz, M. Izadi, Conjugate natural convection of nanofluids inside an enclosure filled by three layers of solid, porous medium and free nanofluid using Buongiorno's and local thermal non-equilibrium models, J. Therm. Anal. Calorim. 135 (2) (2019) 1047–1067.

[6] A.I. Alsabery, E. Gedik, A.J. Chamkha, I. Hashim, Impacts of heated rotating inner cylinder and two-phase nanofluid model on entropy generation and mixed convection in a square cavity, Heat Mass Transfer (2019) 1–18.

[7] A. Alsabery, F. Selimefendigil, I. Hashim, A. Chamkha, M. Ghalambaz, Fluid-structure interaction analysis of entropy generation and mixed convection inside a cavity with flexible right wall and heated rotating cylinder, Int. J. Heat Mass Transf. 140 (2019) 331–345.

[8] A.I. Alsabery, R. Mohebbi, A.J. Chamkha, I. Hashim, Effect of local thermal non-equilibrium model on natural convection in a nanofluid-filled wavy-walled porous cavity containing inner solid cylinder, Chem. Eng. Sci. 201 (2019) 247–263.

[9] A. Alsabery, M. Yazdi, A. Altawallbeh, I. Hashim, Effects of nonhomogeneous nanofluid model on convective heat transfer in partially heated square cavity with conducting solid block, J. Therm. Anal. Calorim. 136 (4) (2019) 1489–1514.

[10] A.I. Alsabery, T. Armaghani, A.J. Chamkha, M.A. Sadiq, I. Hashim, Effects of two-phase nanofluid model on convection in a double lid-driven cavity in the presence of a magnetic field, Int. J. Numer. Methods Heat Fluid Flow 29 (4) (2019) 1272–1299.

[11] A.I. Alsabery, I. Hashim, A.J. Chamkha, H. Saleh, B. Chanane, Effect of spatial side-wall temperature variation on transient natural convection of a nanofluid in a trapezoidal cavity, Int. J. Numer. Methods Heat Fluid Flow 27 (6) (2017) 1365–1384.

[12] A.I. Alsabery, E. Gedik, A.J. Chamkha, I. Hashim, Effects of two-phase nanofluid model and localized heat source/sink on natural convection in a square cavity with a solid circular cylinder, Comput. Methods Appl. Mech. Eng. 346 (2019) 952–981.

[13] A. Alsabery, M. Ismael, A. Chamkha, I. Hashim, Effects of two-phase nanofluid model on MHD mixed convection in a lid-driven cavity in the presence of conductive inner block and corner heater, J. Therm. Anal. Calorim. 135 (1) (2019) 729–750.

[14] E. Jamesahar, M. Ghalambaz, A.J. Chamkha, Fluid–solid interaction in natural convection heat transfer in a square cavity with a perfectly thermal-conductive flexible diagonal partition, Int. J. Heat Mass Transf. 100 (2016) 303–319.

[15] M. Ghalambaz, E. Jamesahar, M.A. Ismael, A.J. Chamkha, Fluid-structure interaction study of natural convection heat transfer over a flexible oscillating fin in a square cavity, Int. J. Thermal Sci. 111 (2017) 256–273.

[16] A. Raisi, I. Arvin, A numerical study of the effect of fluid-structure interaction on transient natural convection in an air-filled square cavity, Int. J. Thermal Sci. 128 (2018) 1–14.

[17] H. Saleh, Z. Siri, I. Hashim, Role of fluid-structure interaction in mixed convection from a circular cylinder in a square enclosure with double flexible oscillating fins, Int. J. Mech. Sci. 161 (2019) 105080.
[18] A. Alsabery, M. Sheremet, M. Ghalambaz, A. Chamkha, I. Hashim, Fluid-structure interaction in natural convection heat transfer in an oblique cavity with a flexible oscillating fin and partial heating, Appl. Therm. Eng. 145 (2018) 80–97.
[19] A.M. Aly, Z. Raizah, Incompressible smoothed particle hydrodynamics simulation of natural convection in a nanofluid-filled complex wavy porous cavity with inner solid particles, Physica A 537 (2020) 122623.
[20] A. Guha, A. Jain, K. Pradhan, Computation and physical explanation of the thermo-fluid-dynamics of natural convection around heated inclined plates with inclination varying from horizontal to vertical, Int. J. Heat Mass Transf. 135 (2019) 1130–1151.
[21] F. Selimefendigil, H.F. Öztop, Fluid-solid interaction of elastic-step type corrugation effects on the mixed convection of nanofluid in a vented cavity with magnetic field, Int. J. Mech. Sci. 152 (2019) 185–197.
[22] K. Kahveci, Numerical simulation of natural convection in a partitioned enclosure using PDQ method, Int. J. Numer. Methods Heat Fluid Flow 17 (4) (2007) 439–456.
[23] A. Kangni, R.B. Yedder, E. Bilgen, Natural convection and conduction in enclosures with multiple vertical partitions, Int. J. Heat Mass Transf. 34 (11) (1991) 2819–2825.
[24] A. Ben-Nakhi, A.J. Chamkha, Conjugate natural convection in a square enclosure with inclined thin fin of arbitrary length, Int. J. Thermal Sci. 46 (5) (2007) 467–478.
[25] A. Ben-Nakhi, A.J. Chamkha, Effect of length and inclination of a thin fin on natural convection in a square enclosure, Numer. Heat Transf. 50 (4) (2006) 381–399.
[26] N. Tatsuo, S. Mitsuhiro, K. Yuji, Natural convection heat transfer in enclosures with an off-center partition, Int. J. Heat Mass Transf 30 (8) (1987) 1756–1758.
[27] S. Acharya, R. Jetli, Heat transfer due to buoyancy in a partially divided square box, Int. J. Heat Mass Transf. 33 (5) (1990) 931–942.
[28] T. Tong, F. Gerner, Natural convection in partitioned air-filled rectangular enclosures, Int. Commun. Heat Mass Transfer 13 (1) (1986) 99–108.
[29] R. Anderson, A. Bejan, Heat transfer through single and double vertical walls in natural convection: theory and experiment, Int. J. Heat Mass Transf. 24 (10) (1981) 1611–1620.
[30] H. Nakamura, Y. Asako, T. Hirata, Natural convection and thermal radiation in enclosures with a partition plate, Trans. JSME 850 (1984) 26472654.
[31] C.-J. Ho, Y. Yih, Conjugate natural convection heat transfer in an air-filled rectangular cavity, Int. Commun. Heat Mass Transf. 14 (1) (1987) 91–100.
[32] M. Parmananda, A. Dalal, G. Natarajan, The influence of partitions on predicting heat transfer due to the combined effects of convection and thermal radiation in cubical enclosures, Int. J. Heat Mass Transf. 121 (2018) 1179–1200.
[33] S. Mehryan, A. Chamkha, M. Ismael, M. Ghalambaz, Fluid–structure interaction analysis of free convection in an inclined square cavity partitioned by a flexible impermeable membrane with sinusoidal temperature heating, Meccanica 52 (11–12) (2017) 2685–2703.
[34] H. Zargartalebi, M. Ghalambaz, A. Chamkha, I. Pop, A.S. Nezhad, Fluid-structure interaction analysis of buoyancy-driven fluid and heat transfer through an enclosure with a flexible thin partition, Int. J. Numer. Methods Heat Fluid Flow 28 (9) (2018) 2072–2088.
[35] R.W. Ogden, Non-linear Elastic Deformations, Courier Corporation, 1997.
[36] J. Donea, A. Huerta, Finite Element Methods For Flow Problems, John Wiley & Sons, 2003.
[37] O.C. Zienkiewicz, R.L. Taylor, P. Nithiarasu, The finite element method for fluid dynamics, The Finite Element Method for Fluid Dynamics, utterworth-Heinemann, 2014.
[38] B. Calcagni, F. Marsili, M. Paroncini, Natural convective heat transfer in square enclosures heated from below, Appl. Therm. Eng. 25 (16) (2005) 2522–2531.
[39] F. Xu, J.C. Patterson, C. Lei, Heat transfer through coupled thermal boundary layers induced by a suddenly generated temperature difference, Int. J. Heat Mass Transf. 52 (21–22) (2009) 4966–4975.
[40] U. Küttler, W.A. Wall, Fixed-point fluid–structure interaction solvers with dynamic relaxation, Comput. Mech. 43 (1) (2008) 61–72.